Rate-independent dissipation and loading direction effects in compressed carbon nanotube arrays

2013 Nanotechnology 24 255707

(http://iopscience.iop.org/0957-4484/24/25/255707)

Nanotechnology **24** (2013) 255707 (10pp) doi:10.1088/0957-4484/24/25/255707

Rate-independent dissipation and loading direction effects in compressed carbon nanotube arrays

J R Raney[1], F Fraternali[2] and C Daraio[3]

[1] Engineering and Applied Science, California Institute of Technology, Pasadena, CA 91125, USA
[2] Department of Civil Engineering, University of Salerno, I-84084 Fisciano(SA), Italy
[3] Department of Mechanical and Process Engineering, ETH Zürich, Switzerland

E-mail: raney@caltech.edu, f.fraternali@unisa.it and daraio@ethz.ch

Received 5 March 2013, in final form 8 May 2013
Published 31 May 2013
Online at stacks.iop.org/Nano/24/255707

Abstract
Arrays of nominally-aligned carbon nanotubes (CNTs) under compression deform locally via buckling, exhibit a foam-like, dissipative response, and can often recover most of their original height. We synthesize millimeter-scale CNT arrays and report the results of compression experiments at different strain rates, from 10^{-4} to 10^{-1} s^{-1}, and for multiple compressive cycles to different strains. We observe that the stress–strain response proceeds independently of the strain rate for all tests, but that it is highly dependent on loading history. Additionally, we examine the effect of loading direction on the mechanical response of the system. The mechanical behavior is modeled using a multiscale series of bistable springs. This model captures the rate independence of the constitutive response, the local deformation, and the history-dependent effects. We develop here a macroscopic formulation of the model to represent a continuum limit of the mesoscale elements developed previously. Utilizing the model and our experimental observations we discuss various possible physical mechanisms contributing to the system's dissipative response.

(Some figures may appear in colour only in the online journal)

1. Introduction

Arrays of nominally-aligned carbon nanotubes (CNTs), or 'CNT forests', have garnered much interest for their use as low-density, compliant (yet thermally and electrically conductive) materials for a variety of applications that have been examined elsewhere [1]. They can be readily synthesized using well-established techniques [2], such as thermal chemical vapor deposition [3]. This has allowed their integration into systems as diverse as field effect transistors [4], thermal heat sinks [5], brushes for electrical motors [6], and fatigue-resistant foams [7].

The mechanical behavior of these systems has been investigated for arrays of varying thicknesses and morphologies [8, 9]. The mechanical response can vary greatly, depending on such factors as CNT diameter distribution [10], CNT surface roughness [11, 12], the density of CNT–CNT contacts [13], and the presence of microstructural heterogeneities [14]. Under compression, the arrays undergo a localized response in which CNTs reorient and form collective buckles [15]. Compression reveals a hysteretic global stress–strain response, exhibiting viscoelasticity [9, 16] and dissipating mechanical energy [17]. The mechanisms of this energy dissipation, which is at least two orders of magnitude greater than that of commercial polymeric foams of comparable density ($\sim$0.2 g cm^{-3}) [18], have remained an area of investigation.

Under compression, CNT arrays exhibit a complex mechanical response. Due to the well-established gradients in physical properties along the direction of CNT alignment in many types of CNT arrays (e.g., gradients in CNT diameter [19], alignment [20], and contamination [21]), a gradient in the mechanical response is observed. Increasing compressive strain is often accommodated by the sequential formation of buckles from the base (i.e., substrate-side) of

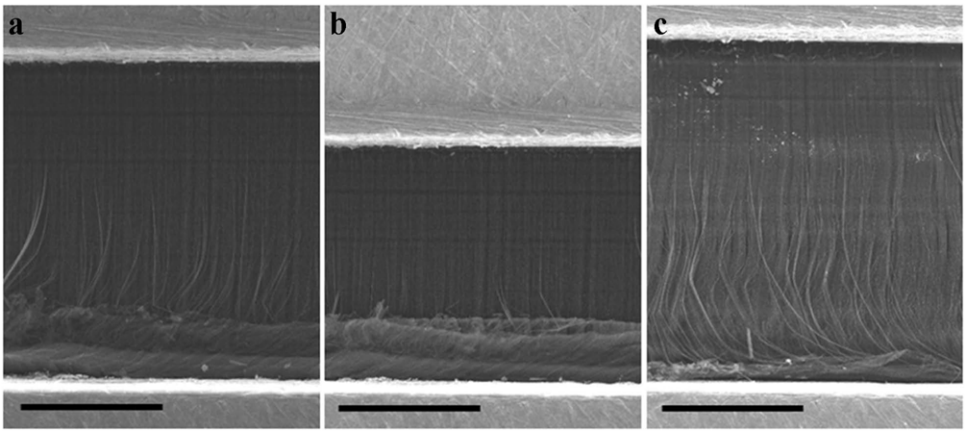

Figure 1. (a) A CNT array in a vise is held at low (∼0.19) compressive strain and (b) at higher (∼0.4) compressive strain, followed by (c) the array after it has recovered some of its original height after release from maximum strain; the scale bars represent 500 μm (horizontal striations arise from slight fluctuations in the input rate of the chemical precursors, as discussed elsewhere [14]).

the array [17], as shown in figure 1. This has been observed regardless of whether or not the array has been physically removed from the substrate used during synthesis [16] or is still attached to it [22].

Several efforts have sought to link the structure of individual CNTs (e.g., diameter or number of walls) or the relative positions of many CNTs to the recoverability of the system after it is compressed [11, 13, 23], and this remains an active area of research. Certain types of CNT arrays (such as those synthesized by vapor phase catalyst systems, as in [17] and as we do here) tend to recover most of their original height upon release of a compressive load, allowing the system to be repeatedly loaded. Figure 2(a) shows the stress–strain response for the first few compressive cycles to a maximum strain of 0.4 (i.e., the sample is deformed a total displacement of 40% of its original height). The primary (first) compressive cycle is indicated by the solid line and the subsequent loading cycles indicated by the dashed lines. Though all compressive cycles are dissipative, as illustrated by the hysteretic response formed by distinct loading and unloading paths, there is a large difference between the stress levels of the first compressive cycle and all of the subsequent cycles. These later cycles differ very little from one to the next, quickly reaching a 'fully-preconditioned' response which remains almost unchanged for dozens or hundreds of cycles [7].

In figure 2(b) the same sample that was compressed to a strain of 0.4 in figure 2(a) is subsequently compressed beyond that previous maximum to a new maximum compressive strain of 0.8. As soon as the strain exceeds the threshold of the previous maximum strain, the material returns to the 'primary loading path' and behaves as though it were not compressed previously. Figure 2(c) shows that combining the response for the first compression from 0 to 0.4 strain with that of the first compression from 0.4 to 0.8 strain results in an uninterrupted path. That is, the material proceeds through a separate preconditioning phase from 0.4 to 0.8 regardless of the earlier preconditioning to 0.4.

The above is a result of the unique mechanism by which these materials locally deform. There is a locality of preconditioning that results from the reorientation of individual CNTs [15] followed by the formation of collective buckles (figure 1). Any time a previous maximum strain is exceeded, local irreversible microstructural rearrangements are necessary to allow the individual CNTs to undergo buckle formation along a portion of the height that has not previously been deformed in any way. This explains why the stress response is forced back to the primary loading path (e.g., the solid line in figure 2(c)) when a pristine portion of the structure is encountered. This combination of effects is analogous to the Mullins effect [24], as observed in rubbers (observed previously in CNT arrays under indentation [25] and compression [26, 27]).

Here, we present several characteristics of CNT arrays. (1) We show that the complex compressive response of CNT arrays described above proceeds independent of strain rate. (2) We discuss the physical anisotropy of the material and how it affects the mechanical response of the system (showing the importance of taking the loading direction into account when designing materials based on CNT arrays for optimal performance in applications such as protective foams). (3) We discuss the experimental observations above in the context of a one-dimensional model based on bistable elements in series that we developed previously [26–28]. The model is able to capture the global stress–strain response of CNT arrays as well as the local deformation that is observed in such systems. We expand on the model here by introducing a 'macroscopic' formulation designed to approximate a continuum limit of the mesoscale elements developed in earlier work. We also examine the physical basis for the choice and effectiveness of the model. (4) We discuss the observed strain rate independence, the anisotropic behavior, and our multiscale model as they relate to mechanisms contributing to dissipation in CNT arrays.

2. Experimental results

We synthesized arrays of nominally-aligned CNTs using a common vapor phase (or 'floating catalyst') procedure that utilized a thermal chemical vapor deposition (CVD)

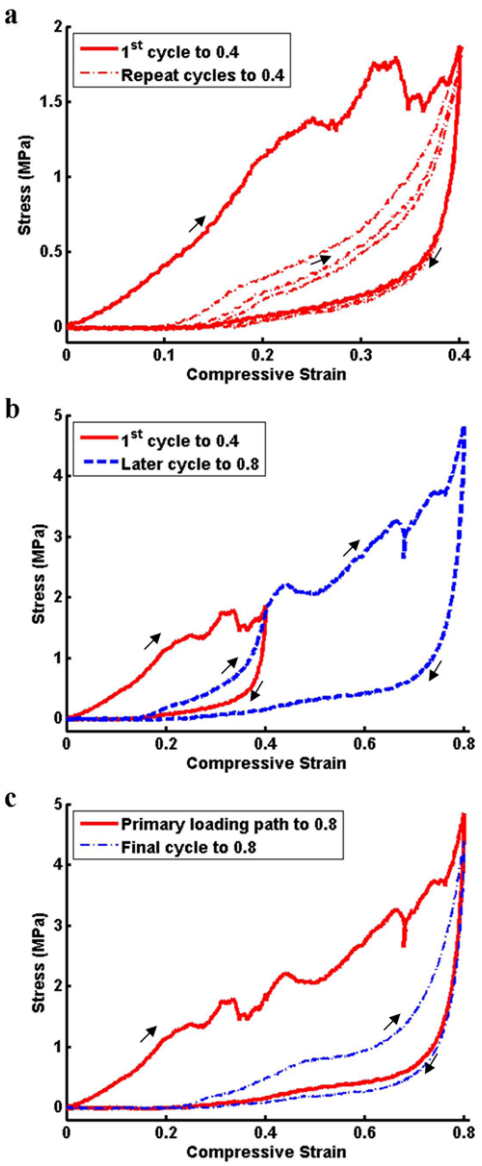

Figure 2. (a) Stress–strain response of the first (solid line) and second to fourth (dashed lines) compressive cycles to 0.4 strain; (b) first (solid line) cycle to 0.4 strain and the fourth cycle (dashed), which was the first cycle beyond 0.4 strain, up to 0.8; (c) the primary loading curve (solid) constructed from part (b), with the stress for strains 0 to 0.4 obtained from the solid line in part (b) and that for strains from 0.4 to 0.8 obtained from the dashed line in part (b); the dashed line in (c) corresponds to a later cycle to 0.8, after the material exhibits a steady-state response.

system [3]. A solution of ferrocene and toluene was made at a concentration of 0.02 g ml^{-1} and injected into the 827 °C heating zone of the CVD furnace at 1 ml min^{-1} using a syringe pump. The ferrocene pyrolyzes in the heating zone to release Fe, which, upon agglomerating into nanoscale particles, acts as the catalyst for CNT growth. The toluene acts as a carbon source. CNT arrays were synthesized to a thickness of approximately 1 mm (which took approximately 50 min) at atmospheric pressure in a flow of gas consisting of either 50% argon and 50% hydrogen or 100% argon, depending on the sample. The CNTs that result are characterized extensively elsewhere (e.g., [10]). The arrays consist of multiwall CNTs of outer diameters of approximately 19 nm and on average 18 concentric walls when hydrogen was used in the flow gas, and approximately 46 nm and 56 walls when no hydrogen was used (ultimately, this affects the bulk mechanical properties, as described in [10]). Samples were subsequently removed from their growth substrates (in approximately 4 × 4 mm^2 samples) using a razor blade and their bulk densities were measured (mass divided by total volume). Quasistatic compression was performed with an Instron E3000. Samples were placed between compression plates such that the direction of nominal CNT alignment either aligned with the direction of compression (the 'parallel' case described later) or perpendicularly to it (the 'perpendicular' case).

We compressed the samples at strain rates from $\dot{\epsilon} = 10^{-4}$ to 10^{-1} s^{-1}. First the samples were compressed three times to a strain of $\epsilon = 0.4$ followed by three compressive cycles to maximum strain $\epsilon = 0.8$ (figure 3). Figure 3(a) shows the stress–strain relationship for the first compressive cycle to strain $\epsilon = 0.8$, after the samples were preconditioned up to strain $\epsilon = 0.4$. As shown in figure 2, this means that up to $\epsilon = 0.4$ the response is that of the preconditioned material and above $\epsilon = 0.4$ the response is that of the pristine material, i.e., along the primary loading path.

Samples at all four strain rates clearly respond very similarly. Importantly, however, as discussed in our previous work [10, 29], the stress response of the samples in compression is linearly dependent on the bulk density of the samples. Though we took the samples used in these tests from directly adjacent portions of their growth substrate, the density varies systematically even within a growth substrate [29]. It is therefore useful to normalize the stress response by sample bulk density, as we have done in figure 3(b) for the data displayed in figure 3(a). Notice that in this case the responses are even more similar, almost entirely covering one another on the plot. This is observed to be true both in the preconditioned region and along the primary loading path. Analogously, we show the stress–strain response after repeated compression (i.e., with the material fully preconditioned all the way up to $\epsilon = 0.8$) and this same data normalized by density in figure 3 panels (c) and (d), respectively. When variations in density are properly accounted for, the quasistatic response is thus observed to proceed independently of strain rate.

One study has found that strain recovery and energy dissipation in compressed CNT arrays depends on the strain rate [30], in contrast with our results (we do not discuss the effect of strain rate on strain recovery in detail here, but we observed no such effect). It is possible that differences between the samples lead to this discrepancy, as these materials are known to vary substantially in their characteristics. Most notably [30], utilized CNT arrays made with a different synthesis process, resulting in CNTs of narrower diameter. Though changes in the ratio of strength of the adhesive forces between CNTs relative to their bending modulus are expected from diameter changes [23], another work in the literature also used narrow diameter CNTs and observed no strain rate dependence during mechanical deformation [31]. The discrepancy could also simply be a

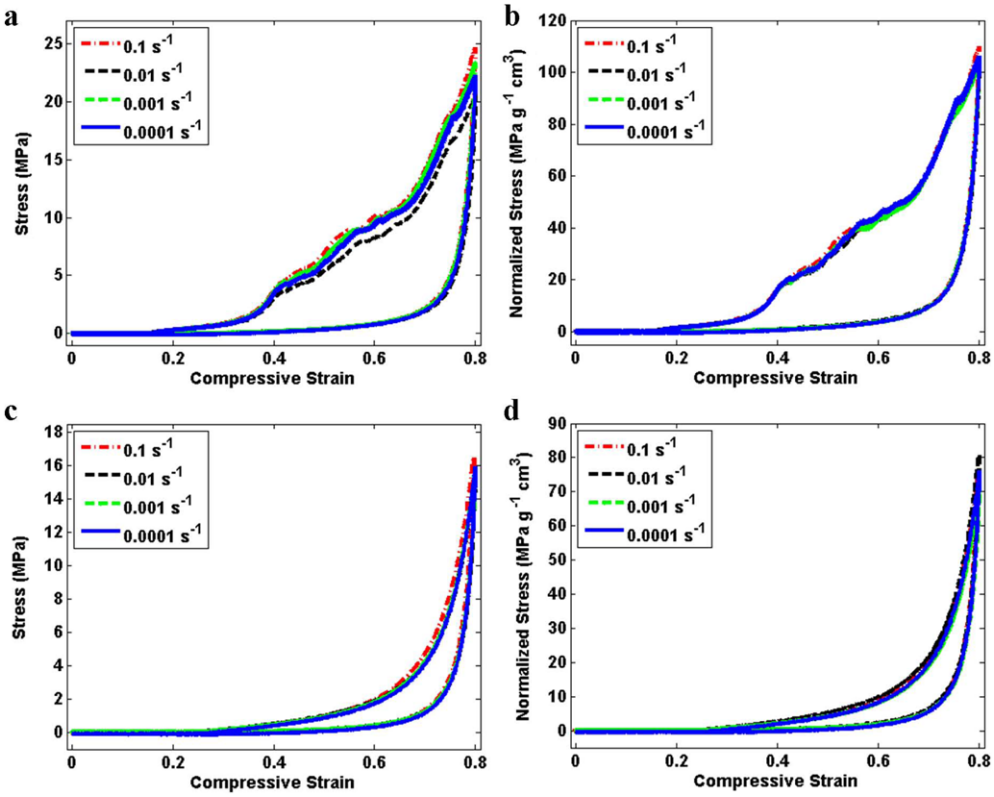

Figure 3. The stress–strain data for CNT arrays compressed from 10^{-4} to 10^{-1} s^{-1}; (a) the first compressive cycles to a strain of 0.8 (with the material already preconditioned up to a strain of 0.4 but pristine above this point); (b) the data of panel (a) normalized by sample density; (c) the compressive cycle after preconditioning to 0.8 strain for each sample; (d) the preconditioned cycles of panel (c) normalized by density.

Table 1. The energy dissipated (proportional to the area enclosed by the hysteresis in the stress–strain curves) and the residual strain after compression for the perpendicular and parallel loading cases shown in figure 4(b) to strain $\epsilon = 0.2$.

Loading case	Dissip. (kJ m^{-3}), Cyc 1	Cyc 2	Cyc 3	Residual strain (%), Cyc 1	Cyc 2	Cyc 3
Perpendicular	22.6	11.8	11.1	2.7	2.7	2.7
Parallel	27.4	9.4	7.3	11	12	12.6

result of variations in density in the samples of the earlier study, which did not account for these. As we have shown previously [29], these density variations greatly affect the mechanical behavior of CNT arrays.

In addition to the quasistatic compression tests, showing independence of the strain rate over the range $\dot{\epsilon} = 10^{-4}$ to 10^{-1} s^{-1}, we have performed limited low-energy impact tests at strain rates in the vicinity of $\dot{\epsilon} = 10^{3}$ s^{-1} [14]. Due to the gap in strain rates between 10^{-4}–10^{-1} and $\sim 10^{3}$ s^{-1} it has remained unclear how to rigorously relate the dissipation observed in quasistatic compression to dissipative parameters, such as the coefficient of restitution, for the case of the impact tests. Establishing additional experimental methods to bridge this gap is an important goal presently being pursued. Regardless, the strain rate invariance over the range of $\dot{\epsilon} = 10^{-4}$–10^{-1} s^{-1} in our samples is in accord with other related work in the literature, such as rate-independent shearing of disordered CNT agglomerates [31] and temperature invariant viscoelasticity of disordered CNT networks over a range of $\sim$1200 °C [32].

Figure 4 and table 1 describe anisotropy effects in relation to the other experimental findings discussed earlier. The alignment of CNT bundles in one direction serves as the obvious physical basis for the notable differences in mechanical response when compressing a CNT array either perpendicular to or parallel with the direction of CNT bundle alignment (see the diagrams in figure 4(a)). Figure 4(b) shows the mechanical response for the two cases, as measured during the compression of sub-samples (taken from the same CNT array sample) to strains of $\epsilon = 0.2$. The thin black lines show the mechanical response after several cycles of compression. This shows similarities and differences between the two directions of compression. In both cases, hysteretic behavior is observed, with the dissipation decreasing from the first to later compressive cycles. Additionally, both samples recover some of their original sizes after compression. However, it is clear that perpendicular compression results in greater recovery from deformation. Table 1 summarizes the plot in figure 4(b). (Similar behavior is observed when the sample is compressed to higher strains, as in figures 4(c) and (d).) Note

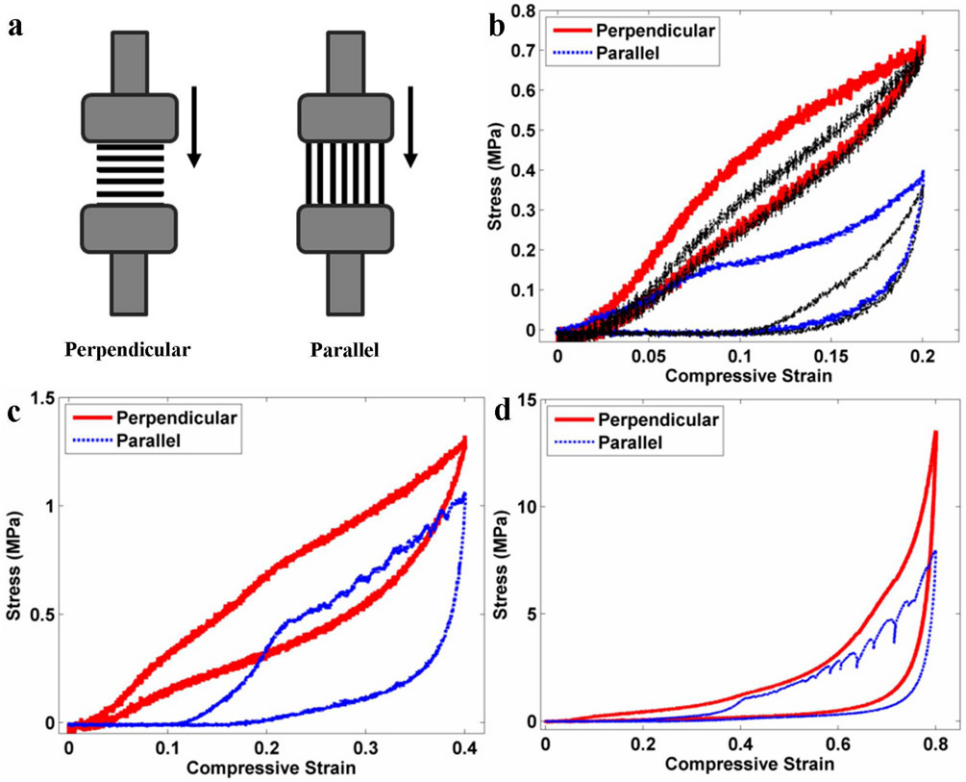

Figure 4. Comparison of the compressive response of CNT arrays that are loaded either perpendicular to (red thick line) or parallel with (blue dotted line) the CNT alignment direction; (a) the orientation of the samples' aligned CNT bundles is indicated by the thick black lines between the compression plates; (b) in this plot the thin black lines show the response of perpendicular and parallel loading after several compressive cycles, revealing that strain recovery is much greater in the perpendicular loading case; (c) the same sample compressed to a strain of $\epsilon = 0.4$ after the compression shown in panel (b); (d) the same sample compressed to a strain of $\epsilon = 0.8$ after the compression shown in panel (c).

that the 'preconditioning' effect discussed earlier, by which the size of the hysteresis and the dissipation that it represents decrease from the first to later cycles, is of greater effect in the parallel loading case. Even though the first compressive cycle dissipates more energy per unit volume in the parallel loading case than in the perpendicular case, by the third cycle this is reversed. Similarly, the residual strain (the amount of the original height never recovered after compression) is larger in the parallel loading case. The implications of the anisotropic behavior are discussed further in section 4.

3. Mechanical modeling

There are several physical observations of CNT arrays that preclude the use of certain simple models (e.g., treating the nominally-aligned CNTs as non-interacting Euler columns) as insufficient in capturing the compressive response. First, as has been repeatedly observed experimentally [15, 17, 22, 26], buckling takes place locally during deformation. Second, there is a physical gradient along the height of the structure for a number of parameters, including the CNT diameters themselves. Third, though at the mesoscale the CNTs (or rather, CNT bundles) are very aligned, at the submicron scale there is extensive lateral entanglement among CNTs [25]. Fourth, there is some evidence in the literature that the rate-independent dissipation observed in CNT arrays (cf section 2) is a result of a timescale mismatch between the internal dissipative mechanisms (e.g., van der Waals interactions, local kinking phenomena, etc) and the external loading [26–28, 31, 33, 34].

For these reasons, the compressive response of CNT arrays is a multiscale dissipative phenomenon, which must be accounted for by models capable of capturing strain localization, material inhomogeneities, and multiple time- and length-scales. The above features are, e.g., captured by multiscale mass–spring models showing bistable elastic behavior at the microscale [26–28]. Such models show two distinct stable phases, which respectively describe the material response before and after buckling, and an intermediate unstable regime associated with snapping events. The mechanical response at the mesoscale is obtained by computing the continuum limit of a chain of infinitely many microscopic springs. In turn, the macroscopic response is described via chains of mesoscopic springs (multiscale behavior).

Preconditioning damage can be easily incorporated by letting a given fraction $\varepsilon_\beta = 1 - \beta$ of microscopic springs exhibit zero stiffness, β denoting an integrity parameter ranging in the interval $[0, 1]$. Such a multiscale model accounts for grading of material properties along the thickness of the structure through anisotropy of material properties at the mesoscopic level. Starting with a 'perfectly

Table 2. Mechanical properties of the single spring models in figure 6 ($\hat{k}_0 = k_0/\rho$ (MPa cm^3 g^{-1})).

Case id	β	$\hat{k}_0$	$(\sigma_C - \sigma_A)/\sigma_A$	ε_A	ε_B	ε_D	k_B/k_0	k_C/k_0
$\parallel$ 0.8	0.86	36.39	−0.575	0.68	0.80	0.43	5.85	57.12
$\parallel$ 0.8(repeat)	0.86	6.52	−0.281	0.68	0.80	0.38	67.41	197.1
$\perp$ 0.4	1.00	15.90	−0.370	0.10	0.40	0.01	1.48	0.04
$\perp$ 0.8	1.00	14.25	−0.505	0.68	0.80	0.50	29.78	102.5

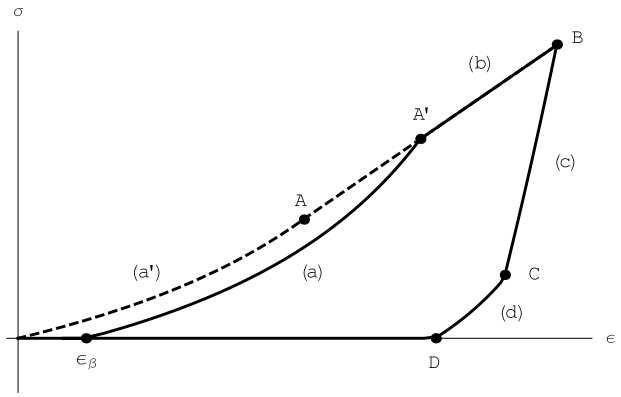

Figure 5. Overall stress–strain response of the present model of a CNT array.

plastic' behavior at the microscopic scale (transformational plasticity), it is worth noting that the multiscale grading of material properties leads to hardening of the overall (macroscopic) stress–strain response [26–28].

In the present work, we describe the mechanical response of a CNT array through the macroscopic stress–strain model mathematically described in the appendix, which aims to represent the continuum limit of a chain of mesoscopic springs defined as in [26, 27]. Such a model is graphically described by the stress–strain plot shown in figure 5, which consists of a closed curve encompassing five different branches and the vertices $O \equiv (0, 0)$; $A_0 \equiv (\varepsilon_\beta, 0)$; $A' \equiv (\varepsilon_{A'}, \sigma_{A'})$; $B \equiv (\varepsilon_B, \sigma_B)$; $C \equiv (\varepsilon_C, \sigma_C)$; and $D \equiv (\varepsilon_D, 0)$. The quantity ε_β represents the activation strain of a previously compressed CNT array (preconditioning 'damage'); while branch $A_0 - A'$ describes the response of the array for small compressive loads, after its activation (phase a); branch A′–B mimics the response of the array in correspondence with the progressive buckling of the tubes (phase b), which is modeled through the continuum limit of a sawtooth diagram featuring infinitesimal stress-drop events (see appendix); the B–C branch describes the initial portion of the unloading phase (c); and the C–D–A_0 branch describes the final portion of such a phase (d). We let $A \equiv (\varepsilon_A, \sigma_A)$ denote the ending point of the particularization of branch (a) for $\varepsilon_\beta = 0$ (branch (a′), cf figure 5). It is possible to characterize the constitutive model given in the appendix through the following independent parameters: ε_β, ε_A, ε_B, ε_D, k_0, k_B, k_C, and $(\sigma_C - \sigma_A)/\sigma_A$, where k_0 and k_C represent the slopes of the branches (a′) and (c) at zero stress, respectively; and k_B represents the slope of the 'buckling' phase (b).

We now employ the constitutive model of figure 5 to fit selected stress–strain plots of CNT arrays loaded either perpendicular to or parallel with the direction of CNT bundle alignment. We let '$\parallel$ 0.8' and '$\parallel$ 0.8(repeat)' denote the stress–strain plots illustrated in figures 3(b) and (d), respectively (i.e., the first loading cycle and a subsequent cycle, respectively, to $\varepsilon = 0.8$ of a CNT array compressed along the direction of CNT alignment). We also let '$\perp$ 0.4' denote the stress–strain plot of a CNT array loaded perpendicular to the direction of CNT bundle alignment up to a maximum strain $\varepsilon = 0.4$, after several preconditioning cycles to $\varepsilon = 0.2$ (first loading cycle to $\varepsilon = 0.4$), corresponding to the 'perpendicular' stress–strain plot shown in figure 4(c). Finally, we let '$\perp$ 0.8' denote the 'perpendicular' stress–strain plot shown in figure 4(d) (i.e. the first loading cycle to $\varepsilon = 0.8$ of a CNT array loaded perpendicular to the direction of CNT bundle, after several preconditioning cycles at $\varepsilon = 0.4$). In each case, we divide the stress σ by the bulk density of the samples (ρ). We perform the fitting of the model in figure 5 to the above stress–strain data via the genetic algorithm procedure described in [28, 35, 36]. Table 2 shows the best fit parameters that we obtained for each of the examined cases, while figure 6 illustrates a comparison between experimental and best fit (model) stress–strain responses. It is worth noting that the best fit models for the parallel loading tests ('$\parallel$ 0.8' and '$\parallel$ 0.8(repeat)') exhibit nonzero activation strain ε_β, as a result of preconditioning damage. In contrast, the perpendicular loading tests ('$\perp$ 0.4' and '$\perp$ 0.8') show zero activation strain. This agrees well with the experimentally-observed differences in strain recovery between the two loading directions. In all cases, we found that material preconditioning reduces the stiffness parameter k_0, and increases the stiffness ratios k_B/k_0 and k_C/k_0.

4. Discussion

As discussed earlier, the present multiscale modeling of CNT arrays accounts for grading of material properties through the thickness of the structure, and the overall hardening-type response (cf figure 6). Of particular relevance is the integrity parameter β, whose introduction is physically motivated by the material structure and response (in addition to the obvious phenomenological motivation). In certain materials, a parameter analogous to β is referred to as a 'damage' parameter. Use of analogous parameters has been used in examinations of biological materials [37], solid rockets [38], and rubber [24]. In all cases, the challenge remains linking the phenomenological 'damage' that is evident in the constitutive response under repeated loading with physical microstructural changes, and in many cases no attempt is made to establish such a link [37–39]. The case of rubber is a rarity in that the physical changes during deformation—such as the 'finite

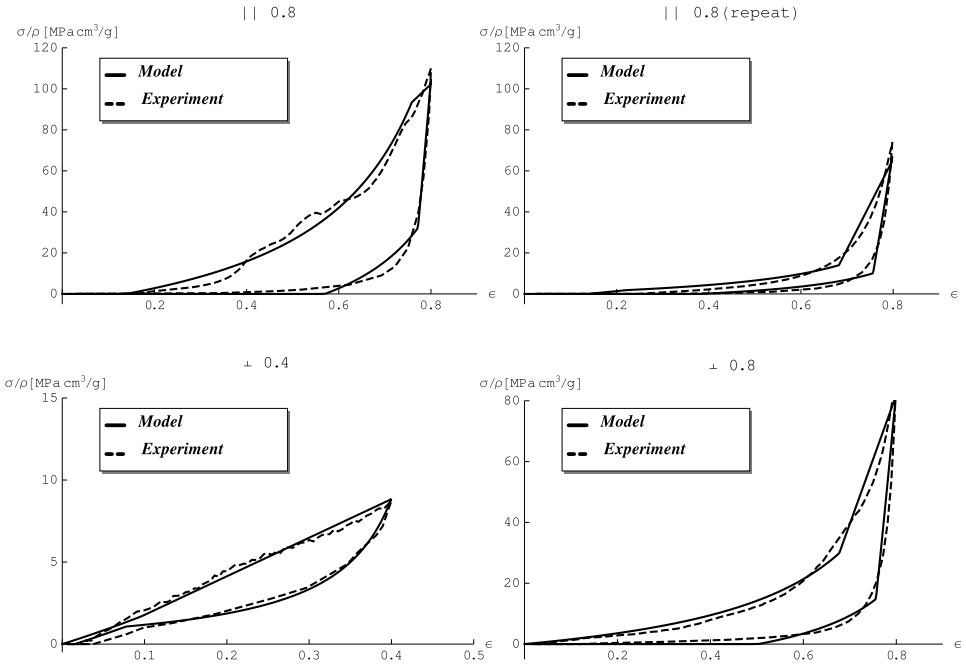

Figure 6. Fitting of stress–strain curves of CNT arrays uniformly compressed either parallel (top) or orthogonal (bottom) to the tube axes.

extensibility' of the individual polymeric chains with resulting damage to the individual chains during tension—are fairly well understood [40], due to its long history of study.

At a phenomenological level, β allows the model to capture with a single parameter the changes that occur to the stress–strain profile after compression, including both the decline in loading stress and the lack of complete recovery. At a more physical level, β relates to the non-reversible reorientation of individual CNTs that occurs prior to buckling [15]. Though the CNT arrays continue to recover much of their height in subsequent cycles, and therefore in an important sense the formation of buckles is reversible, the reorientation of the CNTs that is necessary for the formation of these collective buckles is permanent [15, 17]. It is this latter effect that is being captured by β in our model. The permanent nature of these changes is evidenced both by the significant decrease in the stress from the first to all later cycles, as in figure 2, and by permanent changes in electrical resistance through the thickness of the samples from the first to later cycles, which we have observed previously [18].

Rather than constituting a representation of physical damage, as it might be interpreted in the case of rubber, β is here related to the reordering of CNTs at a microstructural level. That is, β represents structural changes in groups of many CNTs rather than damage to individual CNTs. Through hundreds of observations with SEM and TEM we know that there is statistically no damage to the individual CNTs during quasistatic compression (which is in agreement with the well known extreme bendability of CNTs [41]), and that this is not the cause of the phenomenological changes. Further study is necessary to establish a thoroughly quantitative connection between β and the microstructural reordering.

As noted earlier (section 1), it is clear that the stress–strain response differs from the first compressive cycle to later cycles. The first cycle, during which much more dissipation occurs than in later cycles, involves twisting and reorientation of CNTs [15] (associated with changes in β). Referencing figure 2, it is interesting to note the instabilities reflected in the stress bumps along the primary loading path (i.e., the first time the material is compressed to a particular strain) that are absent entirely from later compressive cycles. The exact pattern of these can vary both in the location and in the extent of the stress leveling/dropoff, depending on inhomogeneities along the height of the structure, which affect buckle formation [14]. This rise and fall in the stress is concomitant with the permanent microstructural rearrangements necessary to allow for the formation of collective buckles [15, 22]. The non-reversible nature of CNT reorientation prior to buckling ensures that this only occurs during the first compressive cycle. The subsequent formation/release of buckles in later cycles can continue for any number of future cycles, but the size of the stress–strain hysteresis reaches a steady-state after a few cycles that does not diminish much with subsequent loading (i.e., β stabilizes).

Figure 4 shows that the stress bumps that are absent after the first parallel loading cycle are also absent when the material is loaded perpendicularly to the long CNT axes (even for the first such cycle). Perpendicular loading does not involve structural buckling, and therefore does not require the realignment of the individual CNTs that leads to the instabilities associated with the rising/falling stress pattern in the primary cycle of parallel loading. These permanent structural changes involved with CNT reorientation and buckling in the parallel loading case explain the poorer strain recovery relative to perpendicular loading.

Because of the large change in response from the first to subsequent cycles it can be difficult for a single model to capture both (see, e.g., the 'idealized Mullins effect' in [42]). It is therefore a strength of the generalized model discussed here that it accounts for the large decline in dissipation from

the first to later cycles without oversimplifying the response of later cycles as non-dissipative.

The model and the experiments also match in their strain rate independence. In the case of the model, it is very clear why this is the case: the timescale of the external loading corresponds to the timescale of the deformation of mesoscopic elements, while the dissipation occurs at the much more rapid timescale of the microscale snapping events. As a result, regardless of the external loading rate, the mesoscopic elements appear static to the snapping events responsible for the dissipation. This is in agreement with our experimental observations of strain rate independence in the quasistatic regime. The authors of a recent study [31] conducted simulations of disordered arrangements of CNTs under deformation in shear. They observed strain rate independent dissipation, with the dominant mechanism being the rapid (sub-nanosecond) breaking and formation of van der Waals interactions between individual CNTs, occurring at a timescale much more rapid than that of external loading. We have shown the same strain rate independent dissipation in our systems and, despite some structural differences between the materials (CNT diameter and alignment, mainly), observe that the same physical mechanism of dissipation would explain the experimental observations provided here.

Early reports of the foam-like energy dissipation of compressed CNT arrays attributed the source of the dissipation to friction between the CNTs and the flow of air through the porous network [17]. Treating a CNT array as an open cell foam, which has been commonly done since first suggested in [17], the latter effect would be expected to have a linear dependence on strain rate [43]. However, we observe no such dependence for our material in the quasistatic regime over several orders of magnitude of strain rates. This and the rapid recovery of the CNT arrays from a compressed state [11, 17] lead us to conclude that viscous flow of air is a negligible source of dissipation in these systems at quasistatic strain rates (for both the primary loading cycle and subsequent preconditioned cycles).

In addition to ruling out viscous dissipation as a major contributor to the response of the system, we also rule out any significant contribution from the permanent damage of individual CNTs. As mentioned earlier, though such an effect might be expected (especially during the first compressive cycle), hundreds of SEM and TEM observations have yielded no evidence of damage to individual CNTs after quasistatic compression (in contrast with impact tests, which have shown the capability to cause damage in individual CNTs [25]). The well known flexibility and recoverability of CNTs [44, 45] supports our experimental observations that quasistatic bending and buckling of CNTs will not cause internal damage.

Individual CNTs of certain types have been shown to form kinks under compression or bending [44, 46, 47]. The kinking involves bending followed by asymmetric kinking associated with negative stiffness and a dissipative response. This would occur at short enough timescales that, similar to the van der Waals interactions described earlier, the resulting dissipative effects would appear rate independent and thereby allow for the 'transformational plasticity' [48] that serves as a motivation for the multiscale bistable spring model that we use. However, despite meeting the timescale requirements, this kinking effect is not expected to provide a significant relative contribution to the overall dissipative response in our system. Moderately thick multiwall CNTs, such as those that make up our samples, predominantly deform via non-dissipative small-amplitude rippling on the inner (compressed) wall rather than via the formation of kinks [49]. We therefore expect that it is the rapid repeated sequence of the van der Waals interactions being broken and reformed that leads to the dissipative response in the CNT arrays studied here (in a similar manner as discussed in [31]) and that these are therefore the physical events that correspond to the microscale spring elements discussed earlier (section 3). Additional experiments are being conducted at higher strain rates to examine where rate dependence might begin. We do, however, expect the rate independence to exist beyond the $\dot{\epsilon} = 10^{-4}$–10^{-1} s^{-1} range of strain rates used here given the nanosecond timescale of the proposed dissipative mechanism.

As a practical matter, notice that for small and moderate strains (figures 4(b) and (c)) the stress rises more rapidly in the perpendicular loading case (i.e., it has a higher modulus). This is an important consideration for use of these materials in engineering applications, particularly as protective foams. Under perpendicular loading the transmitted stress could potentially spike above an application-specific stress threshold if it is particularly low. For applications that will achieve larger strains/stresses, however, it is most probably preferable to use the materials with the CNT axes oriented perpendicular to the stress due to the better CNT recovery and smaller preconditioning effects.

5. Conclusion

The compressive response of CNT arrays was explored, following both experimental and modeling approaches. Experiments show that the quasistatic compressive response is independent of the strain rate from $\dot{\epsilon} = 10^{-4}$ to 10^{-1} s^{-1} when density variations are properly accounted for. We have related this to known rate-independent mechanisms from the literature, particularly the rapid breaking and formation of van der Waals interactions between adjacent CNTs, e.g., as examined by Yang *et al* [31], which occurs at a timescale orders of magnitude shorter than the timescale of external compression. Additionally, we have formulated a macroscopic generalization of the mesoscopic model recently formulated in [26, 27], which is able to reproduce the main features of the experimental response of compressed CNT arrays, including the Mullins-like behavior of the material in repeated compression (which results from the local nature of the buckling and preconditioning), activation effects, and rate-independent dissipation. The effects of loading direction were also considered, which, in addition to contributing to the understanding of the dissipative mechanisms in the material, are of practical relevance to engineering design that could make use of these materials as protective foams. Future work will include a mathematical validation of the 'macroscopic' ansatz illustrated in the appendix (and its generalization to

account for a nonlinear stress–strain response during the buckling phase at very large compressive strains) and an investigation of the dynamic response of CNT arrays, to better understand the response of such structures at high strain rates.

Acknowledgments

FF acknowledges financial support from the University of Salerno through the FARB2012 grant. CD acknowledges support from the Institute for Collaborative Biotechnologies under contract W911NF-09-D-0001 with the Army Research Office.

Appendix. Derivation of the constitutive model

The macroscopic stress–strain response shown in figure 5 originates from multiscale discrete–continuum approaches to the mechanics of CNT arrays, which are based on bistable spring models at the microscale [26, 27]. Figure A.1 shows the overall response of a chain with a finite number of bistable springs as defined in [28], which show increasing values of the 'buckling loads' moving from bottom-to-top of the chain (stress values characterizing the dynamic snaps of the individual microscopic springs from the small-strain stable phase to the post-collapse phase), and the bottom-most spring with zero stiffness (pre-damaged spring). It is seen that such a response exhibits a sawtooth stress–strain diagram characterized by a progressive increase of the stress σ during the spring-collapse events, i.e. a 'hardening-type' buckling response. The limiting stress–strain response of a chain featuring infinitely many springs with graded material properties shows the profile illustrated in figure A.2, in which the microscopic stress drops due to the progressive (bottom-to-top) spring-collapse events have now infinitesimal amplitude and are no longer visible (refer to [26] for details). Such a limiting response characterizes the behavior of the CNT array at the mesoscale. The macroscopic behavior is in turn obtained through the continuum limit of a chain with infinitely many mesoscopic springs, and is represented by the stress–strain response shown in figure 5. The mathematical formulation of the macroscopic stress–strain response is the following:

$$\sigma = \begin{cases} 0, \qquad \text{for } \varepsilon \le \varepsilon_\beta; \\ \sigma^{(a)} = k_0\,(\varepsilon - \varepsilon_\beta)/(1-\varepsilon), \\ \qquad \text{for } (\varepsilon_\beta < \varepsilon < \varepsilon_{A'}) \text{ and } (\text{flag}^{(k-1)} \neq c); \\ \sigma^{(c)} = k_C(\varepsilon - \varepsilon_\beta - \beta\varepsilon_*)/(1-\varepsilon+\beta\varepsilon_*), \\ \qquad \text{for } (\varepsilon_C < \varepsilon < \varepsilon_B) \text{ and } (\text{flag}^{(k-1)} \neq a); \\ \sigma^{(b)} = \sigma_A + k_B(\varepsilon - \varepsilon_A), \\ \qquad \text{for } (\varepsilon_{A'} \le \varepsilon \le \varepsilon_B) \text{ and } (\text{flag}^{(k-1)} = a); \\ \sigma^{(d)} = \max\{k_0(\varepsilon - \varepsilon_D)/(1-\varepsilon),\ 0\}, \\ \qquad \text{for } (\varepsilon < \varepsilon_C) \text{ and } (\text{flag}^{(k-1)} = c); \end{cases} \tag{A.1}$$

where, at the generic step k of a quasistatic loading process, it results $\text{flag}^{(k)} = a$, if $\sigma = \sigma^{(a)}$; $\text{flag}^{(k)} = c$, if $\sigma = \sigma^{(c)}$; $\text{flag}^{(k)} = \text{flag}^{(k-1)}$, otherwise.

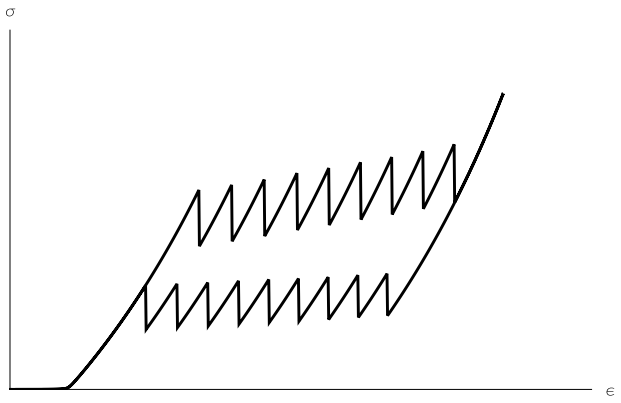

Figure A.1. Overall stress–strain response of a chain of bistable springs with graded mechanical properties along the height of the structure.

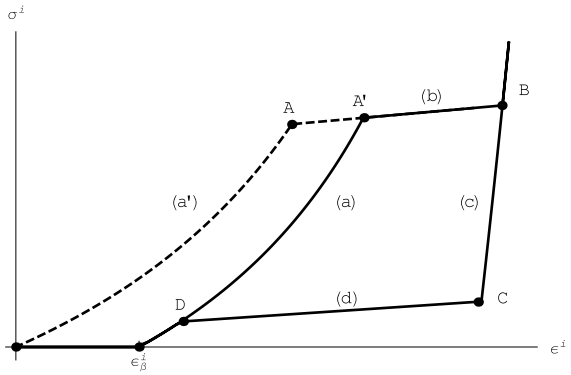

Figure A.2. Limiting response of a chain of infinitely many microscopic springs with graded mechanical properties.

The meaning of the different material parameters appearing in equation (A.1) is provided in section 3.

References

[1] Liu L, Ma W and Zhang Z 2011 *Small* **7** 1504–20
[2] Seah C-M, Chai S-P and Mohamed A R 2011 *Carbon* **49** 4613–35
[3] Andrews R, Jacques D, Rao A M, Derbyshire F, Qian D, Fan X, Dickey E C and Chen J 1999 *Chem. Phys. Lett.* **303** 467–74
[4] Tans S J, Verschueren A R M and Dekker C 1998 *Nature* **393** 49–52
[5] Kordás K, Tóth G, Moilanen P, Kumpumäki M, Vähäkangas J, Uusimäki A, Vajtai R and Ajayan P M 2007 *Appl. Phys. Lett.* **90** 123105
[6] Tóth G, Mäklin J, Halonen N, Palosaari J, Juuti J, Jantunen H, Kordás K, Sawyer W G, Vajtai R and Ajayan P M 2009 *Adv. Mater.* **21** 2054–8
[7] Suhr J, Victor P, Ci L, Sreekala S, Zhang X, Nalamasu O and Ajayan P M 2007 *Nature Nanotechnol.* **2** 417–21
[8] Waters J F, Riester L, Jouzi M, Guduru P R and Xu J M 2004 *Appl. Phys. Lett.* **85** 1787–9
[9] Deck C P, Flowers J, McKee G S B and Vecchio K 2007 *J. Appl. Phys.* **101** 023512
[10] Raney J R, Misra A and Daraio C 2011 *Carbon* **49** 3631–8
[11] Bradford P D, Wang X, Zhao H and Zhu Y T 2011 *Carbon* **49** 2834–41
[12] Li X, Ci L, Kar S, Soldano C, Kilpatrick S J and Ajayan P M 2007 *Carbon* **45** 847–51

[13] McCarter C, Richards R, Mesarovic S, Richards C, Bahr D, McClain D and Jiao J 2006 *J. Mater. Sci.* **41** 7872–8
[14] Raney J R, Wang R Y and Daraio C 2013 *Carbon* **52** 193–200
[15] Zbib A A, Mesarovic S D, Lilleodden E T, McClain D, Jiao J and Bahr D F 2008 *Nanotechnology* **19** 175704
[16] Lattanzi L, Raney J R, De Nardo L, Misra A and Daraio C 2012 *J. Appl. Phys.* **111** 074314
[17] Cao A Y, Dickrell P L, Sawyer W G, Ghasemi-Nejhad M N and Ajayan P M 2005 *Science* **310** 1307–10
[18] Misra A, Raney J R, De Nardo L, Craig A E and Daraio C 2011 *ACS Nano* **5** 7713–21
[19] Li X S, Zhang X F, Ci LJ, Shah R, Wolfe C, Kar S, Talapatra S and Ajayan P M 2008 *Nanotechnology* **19** 455609
[20] Pinault M, Pichot V, Khodja H, Launois P, Reynaud C and Mayne-L'Hermite M 2005 *Nano Lett.* **5** 2394–8
[21] Abbaslou R M M, Soltan J and Dalai A K 2010 *Appl. Catal.* A **372** 147–52
[22] Hutchens S B, Hall L J and Greer J R 2010 *Adv. Funct. Mater.* **20** 2338–46
[23] Ge L, Ci L, Goyal A, Shi R, Mahadevan L, Ajayan P M and Dhinojwala A 2010 *Nano Lett.* **10** 4509–13
[24] Mullins L 1947 *J. Rubber Res.* **16** 275–89
[25] Misra A, Greer J R and Daraio C 2009 *Adv. Mater.* **21** 334–8
[26] Blesgen T, Fraternali F, Raney J R and Daraio C 2013 *Multisc. Model. Simul.* at press
[27] Blesgen T, Fraternali F, Raney J R, Amendola A and Daraio C 2012 *Mech. Res. Commun.* **45** 58–63
[28] Fraternali F, Blesgen T, Amendola A and Daraio C 2011 *J. Mech. Phys. Solids* **59** 89–102
[29] Misra A, Raney J R, Craig A E and Daraio C 2011 *Nanotechnology* **22** 425705
[30] Pathak S, Lim E J, Abadi P P S S, Graham S, Cola B A and Greer J R 2012 *ACS Nano* **6** 2189–97
[31] Yang X, He P and Gao H 2011 *Nano Res.* **4** 1191–8
[32] Xu M, Futaba D N, Yamada T, Yumura M and Hata K 2010 *Science* **330** 1364–8
[33] Raney J R, Fraternali F, Amendola A and Daraio C 2011 *Compos. Struct.* **93** 3013–8
[34] Fraternali F, Raney J R and Daraio C 2013 *Compos. Struct.* **96** 745–50
[35] El Sayed T, Mota A, Fraternali F and Ortiz M 2008 *J. Biomech.* **41** 1458–66
[36] Fraternali F, Marino A, Sayed T E and Cioppa A D 2011 *Mech. Adv. Mater. Struct.* **18** 225–43
[37] Peña E 2011 *J. Mech. Phys. Solids* **59** 1808–22
[38] Gurtin M E and Francis E C 1981 *J. Spacecr. Rockets* **18** 285–6
[39] Ogden R W and Roxburgh D G 1999 *Proc. Math. Phys. Eng. Sci.* **455** 2861–77
[40] Horgan C O, Ogden R W and Saccomandi G 2004 *Proc. R. Soc.* A **460** 1737–54
[41] Falvo M R, Clary G J, Taylor R M, Chi V, Brooks F P, Washburn S and Superfine R 1997 *Nature* **389** 582–4
[42] De Tommasi D and Puglisi G 2006 *J. Rheol.* **50** 495–512
[43] Gibson L J and Ashby M F 1999 *Cellular Solids: Structure and Properties* (Cambridge: Cambridge University Press)
[44] Yakobson B I, Brabec C J and Bernholc J 1996 *Phys. Rev. Lett.* **76** 2511
[45] Pantano A, Parks M, D and Boyce M C 2004 *J. Mech. Phys. Solids* **52** 789–821
[46] Yap H W, Lakes R S and Carpick R W 2007 *Nano Lett.* **7** 1149–54
[47] Yap H W, Lakes R S and Carpick R W 2008 *Phys. Rev.* B **77** 045423
[48] Puglisi G and Truskinovsky L 2005 *J. Mech. Phys. Solids* **53** 655–79
[49] Arroyo M and Belytschko T 2003 *Phys. Rev. Lett.* **91** 215505